JOURNAL OF AIRCRAFT
Vol. 40, No. 3, May–June 2003

Far-Field Drag-Prediction Technique Applied to Wing Design for Civil Aircraft

Jie Li,* Fengwei Li,† and Qin E‡
Northwestern Polytechnical University, 710072 Shaanxi, People's Republic of China

One of the emphases of this paper was the enhancement of drag prediction as well as the decomposition of drag into its physical components. The drag-prediction capability of the improved WBVS code for transonic flow about wing/body combination was verified by two approaches, code to code and code to experiment. The good agreements indicate that the wing body viscous has the capability to assess the aerodynamic performance in the supercritical wing design for civil transport aircraft. Another task of the present study was to redesign a supercritical wing for a new regional jet aircraft by employing the improved code as an analysis tool for wing/body combination. To accomplish this, a geometry-modifying technique was employed to gradually improve the upper- and lower-surface shapes of wing sections.

Nomenclature

C_D	=	total drag coefficient
C_{Di}	=	induced drag coefficient
C_{Dv}	=	viscous drag coefficient
C_{Dw}	=	wave drag coefficient
C_{Fb}	=	friction drag coefficient of fuselage
C_L	=	lift coefficient
C_p	=	pressure coefficient
c	=	local chord
$\bar{c}$	=	mean aerodynamic chord
M	=	Mach number
$\boldsymbol{n}$	=	unit vector normal to σ or Σ
Re	=	Reynolds number based on mean aerodynamic chord
S	=	wing area
T	=	temperature
(u, v, w)	=	Cartesian velocity components
$\boldsymbol{V}$	=	velocity
(x, y, z)	=	Cartesian coordinates, x along streamwise and z spanwise
$\Delta s = s - s_\infty$	=	specific entropy produced by shock
$(\Delta u, \Delta v, \Delta w)$	=	nondimensional perturbation velocity components
ρ	=	density
Σ	=	transverse surface downstream at a distance where there is no streamwise pressure gradient
σ	=	surface of shock wave

Subscripts

n	=	component normal to shock
1	=	conditions just upstream of shock
∞	=	freestream conditions

Received 31 January 2002; presented as Paper 2002-3146 at the 20th Applied Aerodynamics Conference, St. Louis, MO, 24–26 June 2002; revision received 28 November 2002; accepted for publication 15 December 2002.

*Associate Professor, Department of Aircraft Engineering, Xi'an; lijieruihao@163.com.
†Professor, Department of Aircraft Engineering, Xi'an; fwli@nwpu.edu.cn. Member AIAA.
‡Professor, Department of Aircraft Engineering, Xi'an.

Introduction

THE assessment of aerodynamic performance is a very important and demanding task in the design and development process of a civil aircraft. One of the most important parameters in the aerodynamic design process is the lift-to-drag ratio (L/D) in cruising flight condition, which governs the efficiency of an aircraft. Therefore, both the lift and the drag must be accurately predicted in order to be able to maximize L/D of an aircraft by refining and improving its shape.[1]

In general, the lift can be accurately obtained by using Computational-fluid-dynamics (CFD) methods. However, the quality of the drag prediction also plays a key role in the evaluation procedure. This is especially so in the early design stage when various configurations have to be investigated.

However, drag prediction is traditionally a difficult task, both experimentally and numerically, and is one of the major challenges in aerodynamics. In experiments, it is difficult to simulate all of the features of the physical problem, for example, the Reynolds number. Moreover, problems arise as a result of interference effects, in particular with the model support, and because of the difficulty in measuring quantities that are small compared to the others involved in the tests.

From the numerical point of view, even the tremendous progress as a result of the most advanced CFD methods does not ensure drag predictions with sufficient accuracy.[2] The most common technique to calculate the total drag is based on the pressure and skin-friction integration over the aircraft surface. This so-called near-field technique can lead to an inaccurate drag prediction for two main reasons. First, the overall value of the pressure drag coefficient comes about by the near cancellation of a larger force component in the thrust direction and a slightly larger force component in the drag direction.[3] The second reason is related to the numerical viscosity inherent in Euler or Navier–Stokes (NS) methods, which affects the predicted surface pressures especially in the stagnation region near leading edge and in the recovery region near trailing edge. Errors in the predicted pressures in these two regions have little effect on the lift prediction, but significantly affect the drag prediction.[1] It is clear that the near-field technique can be reliable only if the pressure distribution along the surface is predicted both with greater accuracy and detail.[3]

On the other hand, there is a need in aircraft design and analysis to identify the physical sources of drag. The near-field technique does not allow the separation of the drag into its physical components.

A standard alternative to calculating drag is the far-field integration technique from which the total drag can be accurately predicted. The far-field drag analysis also enables the physical drag sources to be identified. This drag breakdown capability is especially important in the design phase when the performance characteristics

of the aircraft are being maximized by refining and improving its shape. The efficiency of this design process can be greatly enhanced when the physical mechanisms, whereby the drag is created, can be identified.[4,5]

In this paper a far-field technique was applied as an improvement to an Euler/boundary-layer code for the purpose of drag prediction in the supercritical wing design for civil transport aircraft. The main advantage of this technique is that no detailed information on the surface geometry of the configuration is required. It also allows for the decomposition of the drag into its physical components, that is, the drag can be expressed as the sum of the following three components: wave drag, induced drag, and viscous drag. This decomposition is useful in formulating techniques for accurately evaluating drag using CFD method.

Another task of the present study was to redesign a supercritical wing for a new regional jet aircraft by using the improved code to assess the aerodynamic performance of the wing/body combination. To accomplish this, a geometry-modifying technique was employed to gradually improve the upper- and lower-surface shapes of wing sections.

Flow Solver

The flowfield solutions for wing/body combination are obtained by Euler/boundary-layer coupled code WBVS. A brief description of this flow solver and the grid-generation technique is presented next. Details of the WBVS code can be found in Ref. 6.

The WBVS is structured to allow the analysis of complex flows in multiple regions. The multiblock O-H type grids are generated with an elliptic grid-generation method that uses a forcing function control technique. A boundary-layer program, which is coupled to the Euler flow solver, uses an integral method to calculate turbulent boundary layers, and thus simulates the viscous effects on the wing.

The capability of the WBVS code for the evaluation of the wing pressure distributions was well described in Ref. 6.

Far-Field Drag Analysis Method

In principle, the far-field drag computation is based on the momentum theorem. However, for the Euler or NS method the straightforward application of the momentum theorem leads only to the total drag, and the drag components cannot be extracted.

The drag decomposition can be achieved by taking into account the second law of thermodynamics, which implies that entropy increases and total pressure decreases only across a shock wave along a streamline of an inviscid nonisentropic flow. It is then possible to show that the drag can be expressed, not exactly but to a very good degree of approximation, as the sum of the following three components[3]:

$$C_D = C_{\mathrm{Dw}} + C_{\mathrm{Di}} + C_{\mathrm{Dv}} \tag{1}$$

These components are briefly described as follows. The detailed derivations of the formulas can be found in Lock.[3]

Wave Drag

Wave drag can be related to the entropy increase across the surface of a shock wave through the Oswatitsch drag integral:

$$D_{\mathrm{wave}} = \frac{T_\infty}{V_\infty} \int_{\mathrm{shock}} \Delta s \rho (\boldsymbol{V} \cdot \boldsymbol{n})\, \mathrm{d}\sigma \tag{2}$$

This expression of the wave drag is obtained by assuming that the static pressure is unmodified far downstream.

In Ref. 3 Lock gives a simple formula for wave drag, which involves only conditions just upstream of the shock. Following Lock, the wave drag coefficient can be expressed in the form

$$C_{\mathrm{Dw}} = \frac{1}{S} \int_{\mathrm{shock}} F(M) \cdot G(M_1, M_{1n})\, \mathrm{d}\sigma \tag{3}$$

$$F = \frac{2}{\gamma} \left(\frac{1 + 0.2 M_\infty^2}{M_\infty} \right)^3 \tag{4}$$

$$G = \frac{1}{2} \frac{M_{1n}}{\left(1 + 0.2 M_1^2\right)^3} \left[7\, \ell n \left(\frac{5 + M_{1n}^2}{6 M_{1n}^2} \right) + 5\, \ell n \left(\frac{7 M_{1n}^2 - 1}{6} \right) \right] \tag{5}$$

Induced Drag

The induced drag can likewise be derived from the momentum theorem by assuming that entropy does not vary along streamlines.

The nondimensional perturbation velocities are

$$\Delta u = (u - u_\infty)/u_\infty, \qquad \Delta v = (v - v_\infty)/u_\infty$$
$$\Delta w = (w - w_\infty)/u_\infty \tag{6}$$

then the induced drag can be expressed as follows[3,4]:

$$D_{\mathrm{induced}} = \frac{\rho_\infty V_\infty^2}{2} \left\{ \int_\Sigma [(\Delta v^2 + \Delta w^2)\boldsymbol{x}]\boldsymbol{n}\, \mathrm{d}\Sigma - \int_\Sigma \left[\left(1 - M_\infty^2\right) \Delta u^2 \boldsymbol{x} \right] \boldsymbol{n}\, \mathrm{d}\Sigma - \int_\Sigma (2 \Delta u \Delta v \boldsymbol{y} + 2 \Delta u \Delta v \boldsymbol{z}) \boldsymbol{n}\, \mathrm{d}\Sigma \right\} \tag{7}$$

Thus, the induced drag coefficient can be expressed as

$$C_{\mathrm{Di}} = \left[2 \Big/ \left(\rho_\infty V_\infty^2 S \right) \right] D_{\mathrm{induced}} \tag{8}$$

Viscous Drag

Because the viscous effects on the wing surfaces are simulated by means of the viscous/inviscid interaction technique in the WBVS code, the viscous drag can be obtained from the boundary-layer parameters.[3,4]

Following Lock, the viscous drag caused by the wing is predicted by first calculating the components of momentum thickness of the boundary layers on both upper and lower surfaces at the wing trailing edge. The local values of viscous drag coefficient $C_{\mathrm{dv}}(z)$ are then obtained by using the method of Squire and Young, modified to allow for the effects of compressibility and trailing-edge sweep.[3,4,7]

Now, the total viscous drag coefficient can be received by integrating the viscous drag contributions along the span direction z:

$$C_{\mathrm{Dv}} = \int_{\mathrm{span}} \frac{c(z)}{\bar{c}} C_{\mathrm{dv}}(z)\, \mathrm{d}z \tag{9}$$

Drag-Predicting Capability of WBVS

Traditionally, the aerodynamic forces have been measured using strain–gauge balances in experiments. This approach is very good for measuring the lift, but the drag of a civil aircraft at typical cruise angles of attack is often more difficult to measure because of the presence of the model sting or support. Moreover, no experimental results are available for the drag components of a wing/body configuration. In this section two approaches were used to verify the drag prediction and breakdown capability of the WBVS code for transonic flow about wing/body combination.

Code-to-Code Comparison

First, a potential flow code coupled with a boundary-layer solution boundary layer wing fuselage was employed to verify the present drag-prediction method. This code is suitable for computing transonic flow over a wing/body combination and takes into consideration the viscous effects on the wing and thin separation zones.

Clearly, there are some limitations in this approach. However, this is a necessary first step in the assessment of the drag-prediction capability for the WBVS code and also gives indications of the

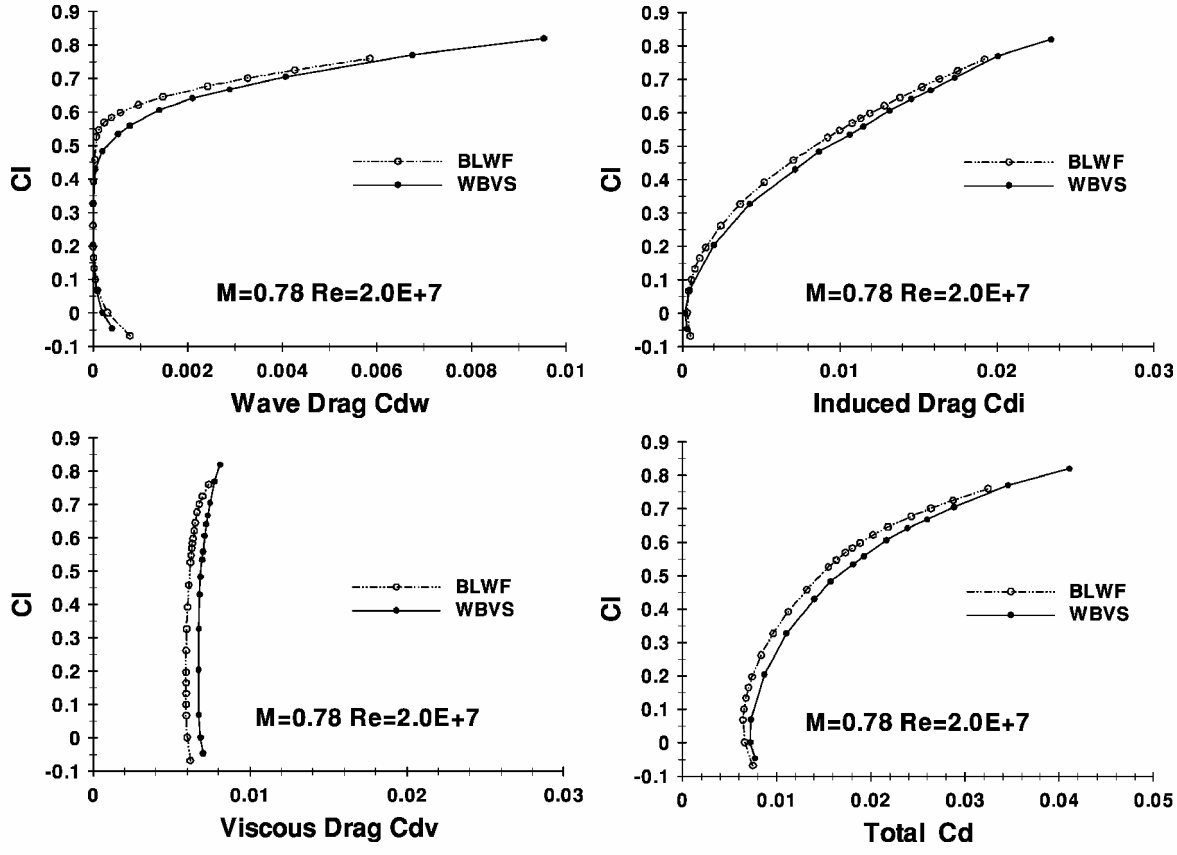

Fig. 1 Comparison of WBVS and BLWF drag results.

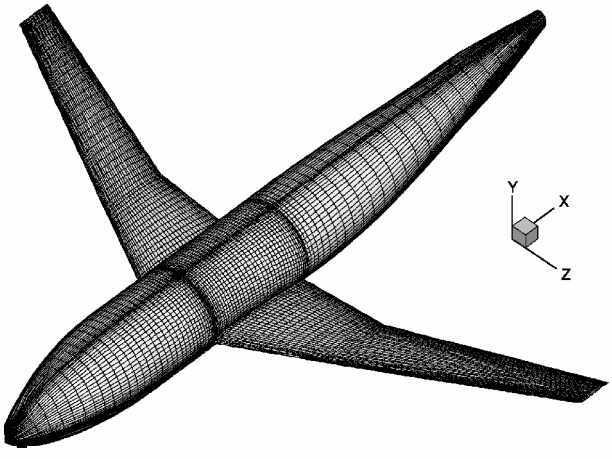

Fig. 2 Surface grid for DLR-F4 wing/body configuration.

computational resources that are required for drag prediction on more complex configurations of engineering interest.

The analysis was carried out by simulating the flow around the AE100 wing/body combination. The results of the WBVS code, in terms of wave drag, induced drag, viscous drag and total drag (not including the friction drag of fuselage), are compared with the BLWF code in Fig. 1. The comparisons demonstrate that the WBVS has the capability to evaluate drag components.

Drag Prediction for DLR-F4 Wing/Body

To further verify the numerical accuracy of the improved WBVS code, the DLR-F4 wing/body configuration[8,9] was used as a test case, to which extensive experimental and CFD studies have been devoted. Figure 2 shows the surface grid of this model. The flow condition selected for this analysis is $M = 0.75$ and $Re = 3.0 \times 10^6$.

Table 1 Computed results about total drag and its components

C_l	C_d	C_{dw}	C_{di}	C_{dv}	C_{Fb}
0.0489	0.01843	0.00013	0.00110	0.00770	0.0095
0.1081	0.01871	0.00005	0.00148	0.00768	0.0095
0.1671	0.01933	0.00005	0.00209	0.00769	0.0095
0.1965	0.01973	0.00005	0.00247	0.00771	0.0095
0.2260	0.02020	0.00005	0.00291	0.00774	0.0095
0.2853	0.02145	0.00014	0.00401	0.00780	0.0095
0.3445	0.02284	0.00022	0.00525	0.00787	0.0095
0.4016	0.02446	0.00027	0.00671	0.00798	0.0095
0.4556	0.02620	0.00031	0.00827	0.00812	0.0095
0.5069	0.02806	0.00038	0.00992	0.00826	0.0095
0.5528	0.03021	0.00051	0.01161	0.00859	0.0095
0.5664	0.03091	0.00054	0.01216	0.00871	0.0095
0.5985	0.03321	0.00131	0.01352	0.00888	0.0095
0.6218	0.03465	0.00167	0.01456	0.00892	0.0095
0.6377	0.03603	0.00224	0.01531	0.00898	0.0095

In Fig. 3 computed pressure distributions are compared with experimental data at various spanwise stations for a lift coefficient of 0.6. Table 1 gives the computed results about the total drag and its components at various lift coefficients, where the component C_{Fb} is obtained with an equivalent fuselage in engineering fashion. The comparison of the computed total drag with experimental data is shown in Fig. 4. The good agreement indicates that the improved code has the capability to assess the aerodynamic performance in the supercritical wing design for civil aircraft.

Wing Design for NRJ Aircraft

About five years ago the AE100 project was proposed for the development of a 100-seat transport aircraft. A supercritical wing was designed, and high-speed wind-tunnel tests were carried out with a wing/body model to confirm the performance of the wing at high Reynolds number. This project was followed by a new project to develop a new regional jet (NRJ) aircraft. In the present work a

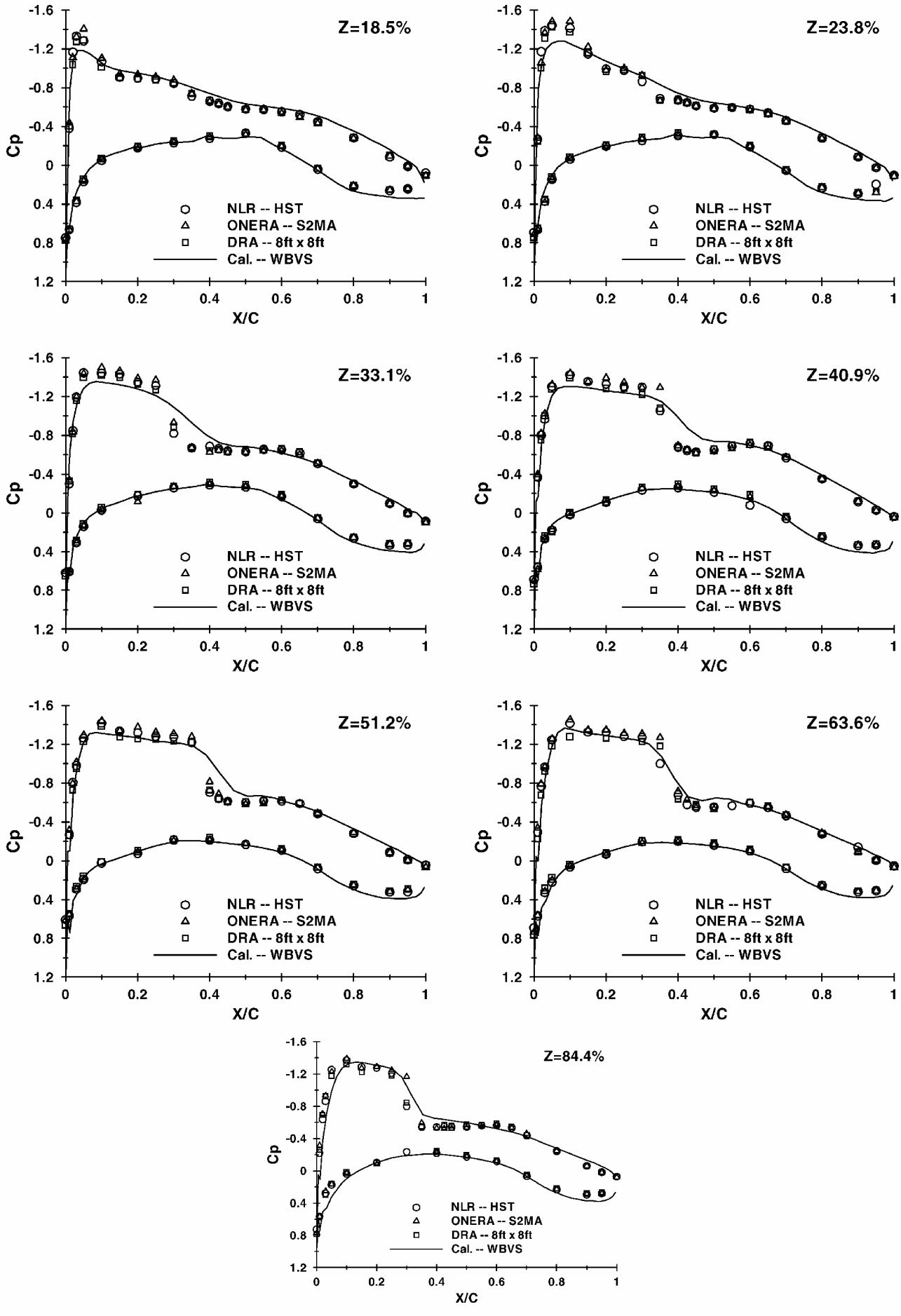

Fig. 3 Comparison of computed and measured pressure distributions at various wing sections for DLR-F4 wing/body configuration.

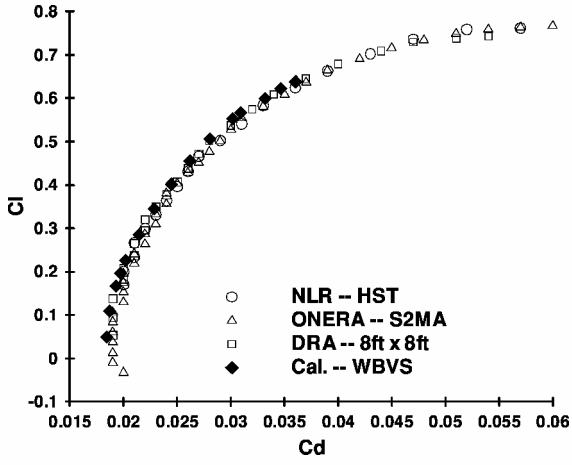

Fig. 4 Comparison of computed total drag with experimental data for DLR-F4 wing/body configuration.

redesign of the supercritical wing based on the AE100 wing using a geometry modifying design technique is made to adapt it for the NRJ.

Main Ideas of Modifying Design Process

According to the design requirements, the area of the high-aspect-ratio supercritical wing for NRJ is 60 m^2, which has been greatly reduced than the 100 m^2 of AE100 wing. Therefore, the mission of current design process is to reproduce wing geometry within manufacturing limits (for example in terms of spar depth and particularly spanwise smoothness) while achieving an optimum aerodynamic performance.

The design of the NRJ transonic wing was carried out in two phases:

1) Several typical airfoil sections located across the span of AE100 wing were chosen to define an initial wing for the NRJ wing planform. The NRJ wing surfaces were linearly lofted between these sections.

2) Careful modifications of defining sections for the supercritical wing were performed to accomplish the design task within constrains especially imposed by structural and operational requirements because of the small wing area.

For the evolving design as modifications to the upper and lower surfaces of wing sections were made, some constraints were prescribed to ensure that the wing remained practical from a structural perspective. These constraints are listed here:

1) Retain the upper surface shape as well as the corresponding pressure distributions resembling as AE100 wing furthest.

2) The physical depth of rear spar at any spanwise station has a reasonable value demanded by actuator sizing and trailing-edge flap design.

3) Between front and rear spars, there would be no significant regions of inflexion, and the available fuel volume would be maintained.

4) Shift the position of the maximum relative thickness backward properly in order to increase the physical thickness at the rear spar.

5) Suitably retain the aft loading inside the kink of the wing if the physical depth of rear spar has a sufficient value.

6) Further weaken the aft loading and hence reduce nose-down pitching moment.

7) Furthermore, the wing is to have a generally smooth and acceptable curvature in both a chordwise and spanwise sense.

The main ideas about current modifications on initial wing are shown in Fig. 5.

In this study wing-section geometries were gradually modified by changing the abscissa at the modification interval according to a stretching function based on a power law. After each modification the new sectional shapes were smoothed using an additional procedure based on Chebyschev polynomial with a least-squares fit in order to make the resulting wing shape amenable for fabrication.

Table 2 Design results about total drag and its components

Wing	C_l	C_d	C_{dw}	C_{di}	C_{dv}	C_{Fb}
Initial	0.5385	0.02443	0.00047	0.01002	0.00674	0.0072
Final	0.5402	0.02460	0.00040	0.01021	0.00679	0.0072

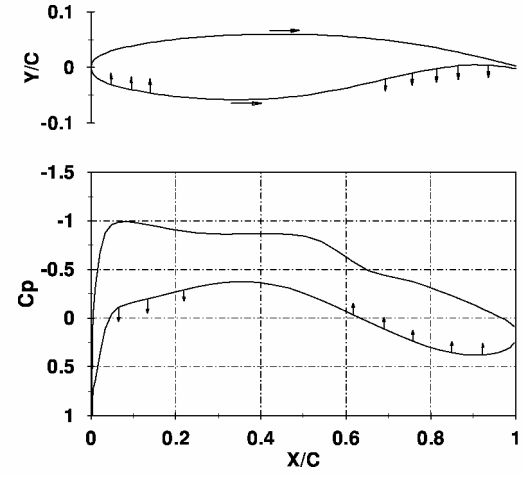

Fig. 5 Guidance of current geometry modifying design.

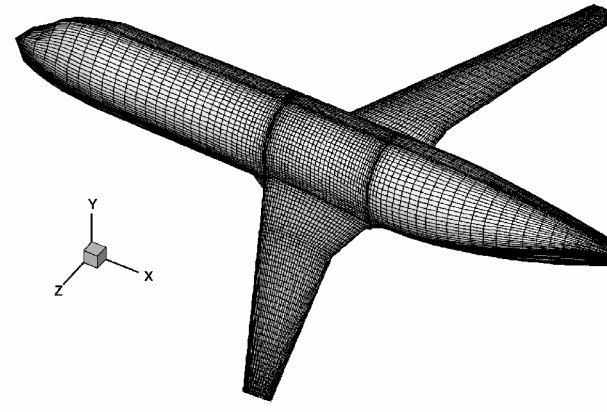

Fig. 6 Surface grid for NRJ wing/body combination.

Design Results and Discussion

The geometry of NRJ wing/body combination is shown by the surface grid in Fig. 6. The design condition selected for this analysis is $M = 0.78$ and $C_l = 0.54$. The Reynolds number is $Re = 1.5 \times 10^7$. Figure 7 shows the sectional geometries of the resulting wing as well as the corresponding pressure distributions after updating the wing sections about 10 adoptable design cycles.

The design results about the total drag and its components are given in Table 2. The order of the drag and its components is reasonable qualitatively. Because of its ability to identify physical drag sources in detail, the far-field drag analysis technique greatly enhanced the design efficiency. What modifications should be made on the wing surfaces was often dependent on the general analysis of drag components in the present design practice.

The changes met the design rules in general. The designed lift-to-drag ratio is about 22, which must be validated by the wind tunnel in next step before the wing goes to application. The front spar depth of the resulting wing was generally reduced because of considerable lower surface changes in the modifying design process.

The aft loading was decreased, and the fore loading was further increased. Hence lesser nose-down pitching moment was obtained.

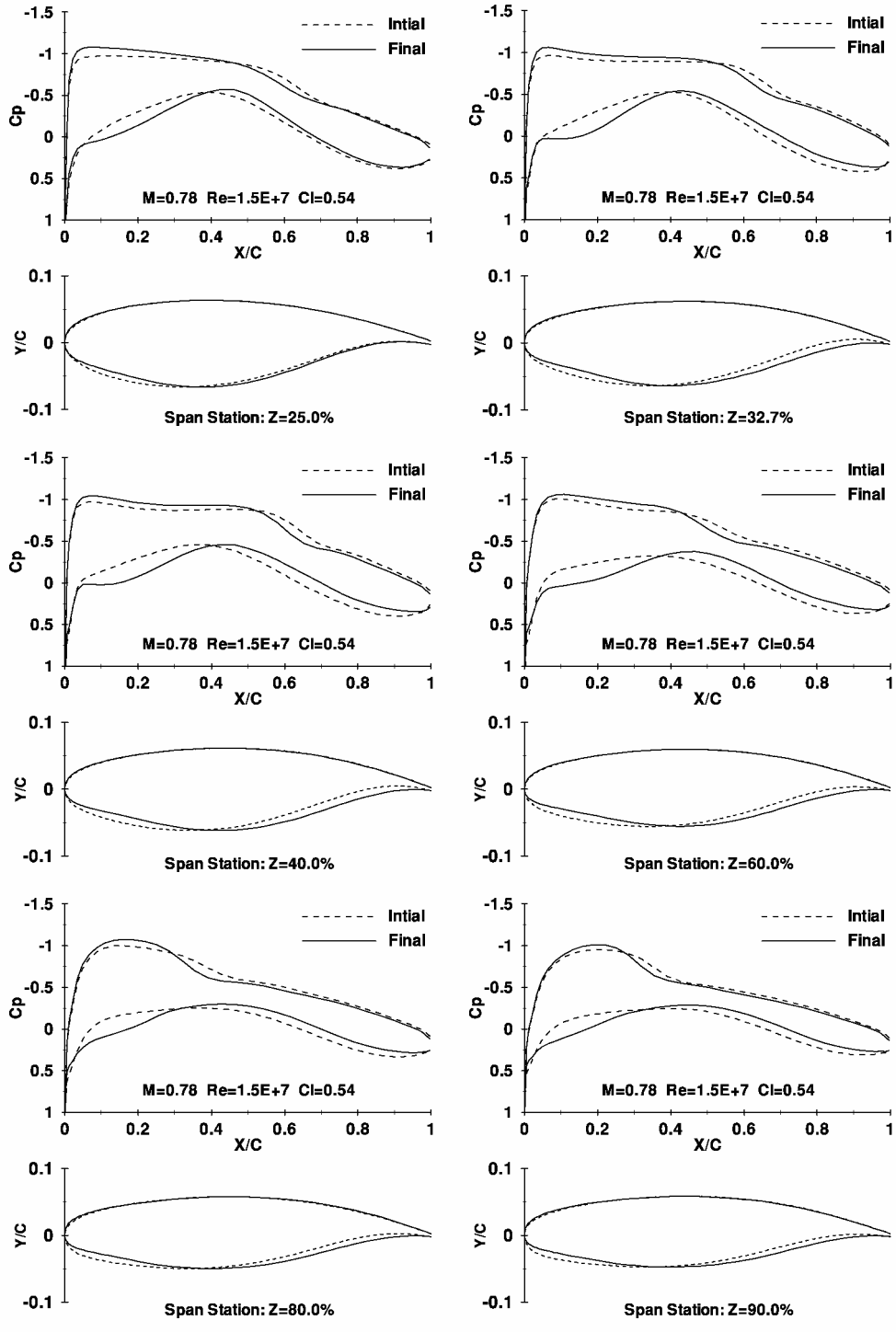

Fig. 7 Comparison of initial and redesigned wing sections.

Conclusions

One objective of this paper was to bring a far-field drag prediction technique into the WBVS code. This method allows the identification of various physical drag sources and can ensure better accuracy than the often-used near-field approach. Furthermore, the far-field approach is less dependent on discretizations and numerical schemes in the Euler solver. This technique allows the aerodynamic designer to gather detailed information on the sources of drag. Therefore, the efficiency of the design process for a civil transport aircraft can be greatly enhanced.

As another task of the present study, a supercritical wing for NRJ aircraft was redesigned by using the improved WBVS code to assess the aerodynamic performance of the wing/body combination. The modifying design exercise described in this paper was restricted mainly to making the wing more practical to structural design.

It must also be emphasized that the present design work is very preliminary. Wing design is an all-around process in which several facets should be coordinated each other for a tradeoff. Further investigation on the NRJ transonic wing is currently underway.

Acknowledgments

This work was supported in part by the fund of "The Developing Program for Outstanding Persons" at Northwestern Polytechnical University for the first author. The authors express their gratitude for the support of this research by Dawei Fu, Jicang Liu, and Qingping

Wang. Many useful discussions with Jiangtao Si are also gratefully acknowledged.

References

[1]van Dam, C. P., and Nikfetrat, K., "Accurate Prediction of Drag Using Euler Methods," *Journal of Aircraft*, Vol. 29, No. 3, 1992, pp. 516–519.

[2]Destarac, D., and Schmitt, V., "Recent Progress in Drag Prediction and Reduction for Civil Transport Aircraft at ONERA," AIAA Paper 98-0137, Jan. 1998.

[3]Lock, R. C., "The Prediction of the Drag of Aerofoils and Wings at High Subsonic Speeds," *Aeronautical Journal*, Vol. 90, No. 896, 1986, pp. 207–226.

[4]Lock, R. C., "Prediction of the Drag of Wings at Subsonic Speeds by Viscous/Inviscid Interaction Techniques," AGARD-R-723, Neuilly-sur-Seine, France, Aug. 1985.

[5]van Dam, C. P., Nikfetrat, K., Wong, K., and Vijgen, P. M. H. W., "Drag Prediction at Subsonic and Transonic Speeds Using Euler Methods," *Journal of Aircraft*, Vol. 32, No. 4, 1995, pp. 839–845.

[6]Li, J., Li, F., and E, Q., "Numerical Simulation of Transonic Flow over Wing-Mounted Twin-Engine Transport Aircraft," *Journal of Aircraft*, Vol. 37, No. 3, 2000, pp. 469–478.

[7]Squire, H. B., and Young, A. D., "The Calculation of the Profile Drag of Aerofoils," Aeronautical Research Council, R&M 1838, London, 1938.

[8]Redeker, G., "DLR-F4 Wing Body Configuration," *A Selection of Experimental Test Cases for the Validation of CFD Codes*, AGARD-AR-303, Neuilly-sur-Seine, France, Vol. II, Aug. 1994, Chap. B.

[9]Redeker, G., Mueller, R., Ashill, P. R., Elsenaar, A., and Schmitt, V., "Experiments on the DFVLR-F4 Wing Body Configuration in Several European Wind Tunnels," AGARD-CP-429, Neuilly-sur-Seine, France, July 1988.